



Nordisk kernesikkerhedsforskning  
Norrænar kjarnöryggisrannsóknir  
Pohjoismainen ydinturvallisuustutkimus  
Nordisk kjernesikkerhetsforskning  
Nordisk kärnsäkerhetsforskning  
Nordic nuclear safety research

NKS-219  
ISBN 978-87-7893-289-1

---

# In-vessel Coolability and Steam Explosion in Nordic BWRs

Weimin Ma, Roberta Hansson, Liangxing Li, Pavel Kudinov,  
Francesco Cadinu, Chi-Thanh Tran

Royal Institute of Technology (KTH), Sweden

March 2010

## Abstract

The INCOSE project is to reduce the uncertainty in quantification of steam explosion risk and in-vessel coolability in Nordic BWR plants with the cavity flooding as a severe accident management (SAM) measure. During 2009 substantial advances and new insights into physical mechanisms were gained for studies of: (i) in-vessel corium coolability – development of the methodologies to assess the efficiency of the control rod guide tube (CRGT) cooling as a potential SAM measure; (ii) debris bed coolability – characterization of the effective particle diameter of multi-size particles and qualification of friction law for two-phase flow in the beds packed with multi-size particles; and (iii) steam explosion – investigation of the effect of binary oxides mixture's properties on steam explosion. An approach for coupling of ECM/PECM models with RELAP5 was developed to enhance predictive fidelity for melt pool heat transfer. MELCOR was employed to examine the CRGT cooling efficiency by considering an entire accident scenario, and the simulation results show that the nominal flowrate (~10kg/s) of CRGT cooling is sufficient to maintain the integrity of the vessel in a BWR of 3900 MWth, if the water injection is activated no later than 1 hour after scram. The POMECO-FL experimental data suggest that for a particulate bed packed with multi-size particles, the effective particle diameter can be represented by the area mean diameter of the particles, while at high velocity ( $Re > 7$ ) the effective particle diameter is closer to the length mean diameter. The pressure drop of two-phase flow through the particulate bed can be predicted by Reed's model. The steam explosion experiments performed at high melt superheat (>200°C) using oxidic mixture of  $WO_3$ -CaO didn't detect an apparent difference in steam explosion energetics and preconditioning between the eutectic and non-eutectic melts. This points out that the next step of MISTEE experiment will be conducted at lower superheat.

## Key words

severe accident, debris coolability, steam explosion

NKS-219  
ISBN 978-87-7893-289-1

Electronic report, March 2010

NKS Secretariat  
NKS-776  
P.O. Box 49  
DK - 4000 Roskilde, Denmark

Phone +45 4677 4045  
Fax +45 4677 4046  
www.nks.org  
e-mail nks@nks.org

Contract AFT/NKS-R(09)75/3

***Midterm Report***

**In-vessel Coolability and Steam  
Explosion in Nordic BWRs**

*Weimin Ma, Roberta Hansson, Liangxing Li, Pavel Kudinov,  
Francesco Cadinu, Chi-Thanh Tran*

Division of Nuclear Power Safety  
Department of Physics  
Royal Institute of Technology (KTH)

April 2010

## Executive Summary

The INCOSE project is to reduce the uncertainty in quantification of steam explosion risk and in-vessel coolability in Nordic BWR plants with the cavity flooding as a severe accident management (SAM) measure.

During 2009 substantial advances and new insights into physical mechanisms were gained for studies of: (i) in-vessel corium coolability – development of the methodologies to assess the efficiency of the control rod guide tube (CRGT) cooling as a potential SAM measure; (ii) debris bed coolability – characterization of the effective particle diameter of multi-size particles and qualification of friction law for two-phase flow in the beds packed with multi-size particles; and (iii) steam explosion – investigation of the effect of binary oxides mixture's properties on steam explosion. An approach for coupling of ECM/PECM models with RELAP5 was developed to enhance predictive fidelity for melt pool heat transfer. MELCOR was employed to examine the CRGT cooling efficiency by considering an entire accident scenario, and the simulation results show that the nominal flowrate (~10kg/s) of CRGT cooling is sufficient to maintain the integrity of the vessel in a BWR of 3900 MWth, if the water injection is activated no later than 1 hour after scram. The POMECO-FL experimental data suggest that for a particulate bed packed with multi-size particles, the effective particle diameter can be represented by the area mean diameter of the particles, while at high velocity ( $Re > 7$ ) the effective particle diameter is closer to the length mean diameter. The pressure drop of two-phase flow through the particulate bed can be predicted by Reed's model. The steam explosion experiments performed at high melt superheat ( $>200^{\circ}\text{C}$ ) using oxidic mixture of  $\text{WO}_3\text{-CaO}$  didn't detect an apparent difference in steam explosion energetics and preconditioning between the eutectic and non-eutectic melts. This points out that the next step of MISTEE experiment will be conducted at lower superheat.

# Contents

Executive Summary .....	2
1. Introduction .....	4
2. Results and Analysis .....	4
2.1. In-vessel coolability .....	4
2.1.1. The effectiveness of CRGT cooling .....	4
2.1.2. Coolability of in-vessel debris bed .....	6
2.2. Steam explosion energetics .....	15
2.2.1. Bubble and melt dynamics .....	18
2.2.2. Steam explosion energetics .....	24
2.2.3. Metallic (tin) versus Oxidic ( $\text{WO}_3$ -CaO) materials .....	25
3. Concluded Remarks .....	26
References .....	27

# 1. Introduction

The goal of the severe accident research at Kungliga Tekniska Högskolan (KTH) is to create knowledge base for resolution of two long-standing severe accident issues, namely steam explosion and corium coolability in severe accident scenarios of Nordic BWRs which adopt cavity flooding as the cornerstone of Severe Accident Management (SAM) measures.

For this objective, the research project INCOSE (In-vessel Coolability and Steam Explosion in Nordic BWRs) is focused on two areas of highest return: (i) in-vessel coolability with severe accident management (SAM) action (e.g., CRGT cooling) since it has more chances to contain the corium in the reactor pressure vessel (RPV), and (ii) steam explosion energetics in case of vessel failure, which may threaten the containment integrity.

This report summarizes the progress and achievements of the project during Year 2009. The research activity has a synergic collaboration with Swedish APRI-7 research program, EU SARNET2 Excellence Network for severe accident research and OECD SERENA-II project dedicated to understanding of steam explosion in reactor safety.

## 2. Results and Analysis

### 2.1. In-vessel coolability

The in-vessel coolability study at KTH is focused on *a*) quantification of the effectiveness of control rod guide tubes (CRGT) cooling as a potential severe accident management (SAM) measure in BWRs; *b*) reduction of the uncertainty in coolability analysis of a debris bed formed in the RPV during a postulated severe accident.

#### 2.1.1. The effectiveness of CRGT cooling

To perform a mechanistic multi-dimensional analysis of heat transfer in the corium-filled lower head, Effective Convective Model (ECM) and Phase-change Effective Convective Model (PECM) were developed at KTH [1-5], which incorporate the advantages of the modern CFD method and the available correlation-based method, being able to simulate melt pool behavior in a complex geometry as the BWR's lower plenum with a forest of CRGTs.

The ECM and PECM were applied to simulation and analysis of melt pool heat transfer in the lower plenum during a severe reactor accident of a BWR of 2500 MW<sub>th</sub>. The key findings are as follows [5]: In case of formation of melt pool with a thickness (height, or depth) less than 0.7 m in the BWR lower plenum, the CRGT cooling at nominal water flow rate, i.e. 62.5 g/sec per CRGT, is sufficient to remove the decay heat generated in the melt pool, and protect the vessel wall from thermal attack. In the case of a melt pool with depth higher than 0.7 m, the CRGT cooling is insufficient, and the vessel wall is predicted to fail in the section connected to the uppermost region of the melt pool; Additional cooling measure (e.g. external cooling, and/or increase of CRGT water flow rate) is needed for protection of the vessel from failure. The ECM/PECM simulation results and key findings suggest that CRGT cooling possesses a high potential as an effective and reliable

mechanism to remove the decay heat from a melt pool formed in the BWR lower plenum. Thus, the CRGT cooling presents a credible candidate for implementation as a SAM measure in BWRs.

During 2009, further work on extension and enhancement of the ECM/PECM predictive capabilities was performed [6-7]. ECM/PECM models for simulations of molten metal layer heat transfer are developed in [6] for consideration of scenario with stratified melt pool heat transfer with CRGT cooling. The PECM simulation results revealed no focusing effect in the metal layer on top of a debris pool formed in a BWR lower plenum [6] in presence of CRGT cooling. On the other hand, very high heat fluxes were obtained on the surface of the CRGTs during rapid solidification of the metal layer. The reason for that was the fixed temperature boundary condition on the inner side of the CRGTs which didn't take into account properly feedback between inner and outer heat transfers in this particular case. In order to capture this feedback, a method has been developed [7] for coupled simulations of the melt pool heat transfer (with PECM model) and the flow and heat transfer inside the CRGTs (with the system thermal-hydraulic code RELAP5). The PECM model of the metal layer heat transfer, implemented on the base of the CFD code Fluent, calculates the transient heat fluxes on the CRGTs walls to be used, as a boundary condition, by RELAP5. Conversely, RELAP5 provides the temperature of the CRGTs external wall as a boundary condition for the simulation of the core melt heat transfer. The coupling between the two codes, which run concurrently, is performed by a scripting interface that organizes the exchange of information at each time step of the PECM simulation (Fig. 1).

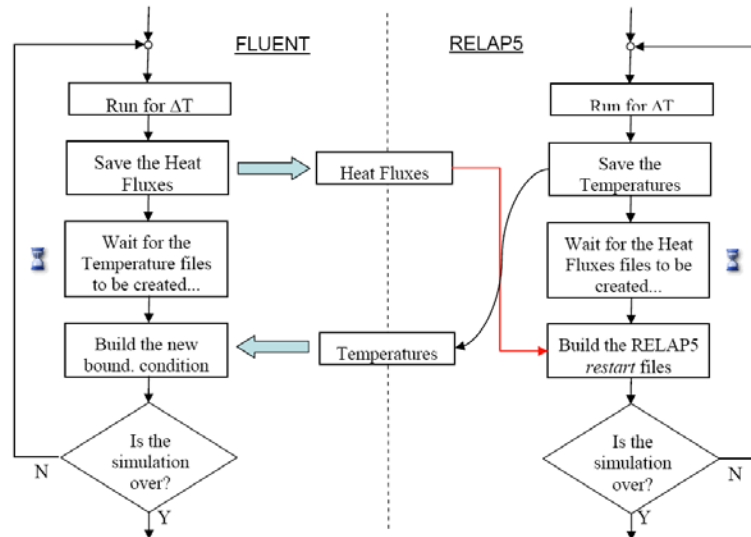


**Fig. 1:** Implementation of the ECM/RELAP5 coupling scheme.

The coupled PECM/RELAP5 simulations results suggest that even in the case of remote, hypothetically bounding scenario of initially hot (2000K) heterogeneous melt pool configuration, with liquid metal layer floating atop of a debris bed, just a fourfold increase of the standard mass flow rate of the CRGT flow appears to be sufficient to prevent CRGT creep. More detailed results can be found in [7].

While the ECM/PECM method provides an efficient and computationally affordable tool for mechanistic multi-dimensional analysis of melt pool heat transfer in the lower head, the effects of system dynamics and accident progression on melt pool heat transfer were not directly considered in the analysis. The influence of coolant injection on other phenomena

was also neglected. This is because ECM/PECM simulations were only focused on the melt pool in the lower head, without any link and interactions with other systems and phenomena. For instance, the core degradation and relocation are important for resulting melt pool in the lower plenum. But this cannot be captured in the ECM/PECM method; instead the boundary conditions (e.g., melt mass, compositions and initial temperatures) have to be assumed in the analysis. To lift this limitation, the whole accident progression (from core degradation, to melt relocation, and to melt pool formation in the lower head) must be simulated. Such a systematic analysis is realized here by using MELCOR code for the severe accident simulation [8]. Based on the MELCOR simulation results, the following points can be concluded.

- The nominal flowrate (~10kg/s) of CRGT cooling is sufficient for in-vessel coolability and to maintain the integrity of the vessel in a BWR of 3900 MWth, if the water injection is activated no later than 1 hour after scram.
- For late recovery of CRGT cooling (later than 1 hour after scram), a higher flowrate than the nominal is needed to contain the melt in the vessel. In case the water injection to the CRGTs is activated in 2 hours, for instance, much higher flowrate (~40kg/s) is required for in-vessel coolability and retention.

Although we are aware of the limitation of MELCOR modeling for melt pool heat transfer in the lower plenum, the first-cut analysis in the present study highlights the importance of timing and flowrate of the CRGT cooling when chosen as a SAM measure for in-vessel corium coolability and retention. For early actuation of the CRGT cooling, there is little corium relocated to the lower plenum for melt pool formation and the prediction by MELCOR code at system level is therefore more credible. For late recovery of the CRGT cooling, a mechanistic multi-dimensional analysis of heat transfer in the corium-filled lower plenum is necessary for confirmation and quantification. This is why we at KTH developed the Effective Convective Model (ECM) for simulation of corium behavior in a complex geometry like the BWR's lower plenum with a forest of CRGTs. The next step is to complete methodology formulation for information transfer from MELCOR output to the ECM method, and to perform ECM analysis for the late injection scenarios. The dual approach leverages on the strength of the two methods (MELCOR/ECM), and therefore increases the reliability of the assessment.

### **2.1.2. Coolability of in-vessel debris bed**

The research on this topic is concerned with reducing the uncertainty in coolability analysis of a debris bed which may be formed from fuel coolant interactions (FCIs) in the reactor pressure vessel (RPV) during various stages (cf. Fig. 2a & 2b) of a severe accident scenario. Due to its internal pores which facilitate coolant ingress, the debris bed provides more chances to remove the decay heat than a molten corium pool where coolant access is very limited (only to surface). Thus, debris bed coolability plays an important role in the termination and stabilization of a severe accident.

Towards the quantitative understanding of debris bed coolability, many experiments [9-14] have been conducted to investigate two-phase flow and heat transfer in particle beds. We at KTH also addressed the influences of the bed's characteristics (prototypicalities) on coolability [15]. To analyze the experiments and finally assess debris coolability in reactor application, a great number of analytical models and empirical correlations were developed

for prediction of two-phase flow (friction) and heat transfer (dryout heat flux) in packed beds. The central point in modeling was to provide the formulation of the friction laws for momentum equations of single and two-phase flow in porous media.

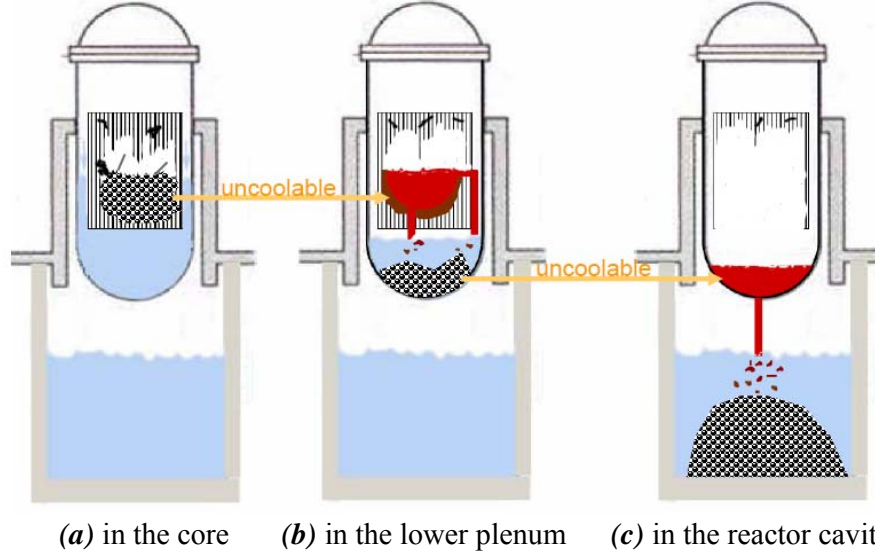


**Fig. 2:** Debris bed formation during different stages of a severe accident scenario.

The momentum equation of single-phase flow through porous media can be expressed by Ergun's equation [16]:

$$-\frac{dp}{dz} = \frac{\mu}{K} J + \frac{\rho}{\eta} J^2 \quad (1)$$

where  $dp/dz$  is the pressure gradient along the bed,  $\varepsilon$  is the porosity,  $\mu$  is the dynamic viscosity of fluid,  $d$  is the diameter of particles,  $\rho$  is the density of the fluid and  $J$  is the superficial velocity of fluid. For uniform spherical particles bed, the permeability  $K$  and passability  $\eta$  are taken as

$$K = \frac{\varepsilon^3 d^2}{150(1-\varepsilon)^2} \quad \eta = \frac{\varepsilon^3 d}{1.75(1-\varepsilon)} \quad (2)$$

where,  $d$  and  $\varepsilon$  are particle diameter and porosity of the debris bed, respectively.

Ergun's equation was adapted to two-phase flow in porous media by the inclusion of relative permeability, relative passability and interfacial friction:

$$-\frac{dp_l}{dz} = \rho_l g + \frac{\mu_l}{K \cdot K_{r,l}} J_l + \frac{\rho_l}{\eta \cdot \eta_{r,l}} J_l \cdot |J_l| - \frac{F_i}{1-\alpha} \quad (3)$$

$$-\frac{dp_g}{dz} = \rho_g g + \frac{\mu_g}{K \cdot K_{r,g}} J_g + \frac{\rho_g}{\eta \cdot \eta_{r,g}} J_g \cdot |J_g| + \frac{F_i}{\alpha} \quad (4)$$

where  $J_l$  and  $J_g$  are the superficial velocities of fluids; and  $K_r$  and  $\eta_r$  are relative permeability and relative passability that differ from model to model as listed in Table 1, where the interfacial friction  $F_i$  is also defined.

Table 1. Relative permeability and passability in models for coolability analysis.

<b>Parameter Model</b>	$K_r$	$\eta_r$	$F_i$
Lipinski (1981) [17]	$K_{r,l}=s^3$ $K_{r,g}=\alpha^3$	$\eta_{r,l}=s^3$ $\eta_{r,g}=\alpha^3$	0
Reed (1982) [18]	$K_{r,l}=s^3$ $K_{r,g}=\alpha^3$	$\eta_{r,l}=s^5$ $\eta_{r,g}=\alpha^5$	0
Hu & Theofanous (1991) [13]	$K_{r,l}=s^3$ $K_{r,g}=\alpha^3$	$\eta_{r,l}=s^6$ $\eta_{r,g}=\alpha^6$	0
Schulenberg & Müller (1987) [19]	$K_{r,l}=s^3$ $K_{r,g}=\alpha^3$	$\eta_{r,l}=s^5$ $\eta_{r,g}=\alpha^6, \alpha>0.3$ $\eta_{r,g}=0.1\alpha^4, \alpha\leq 0.3$	$F_i = 350s^7 \alpha \frac{\rho_l K}{\eta \sigma} (\rho_l - \rho_g) g \left( \frac{J_g}{\alpha} - \frac{J_l}{s} \right)^2$

From the above equations, one can see the particle diameter is an important parameter to determine flow friction (and therefore dryout heat flux) of a porous bed. Nevertheless, the identification of particle diameter is not straightforward when the bed is composed of multi-diameter particles, as the case for reactor application where the debris particles have a wide range of size distribution.

For the mixture of particles with a size distribution, the mean particle diameter is very different even for the same combination of multi-size spheres, depending on which size distribution function (mass, area, length, number, etc.) to be chosen [20]. Accordingly, there exist among others the mass mean diameter, area mean diameter, length mean diameter and number mean diameter, defined as follows.

$$d_m = \sum x_i m_i = \sum \left( x_i \frac{x_i^3 f_i}{\sum x_i^3 f_i} \right) = \frac{\sum x_i^4 f_i}{\sum x_i^3 f_i} \quad (5)$$

$$d_a = \sum x_i a_i = \sum \left( x_i \frac{x_i^2 f_i}{\sum x_i^2 f_i} \right) = \frac{\sum x_i^3 f_i}{\sum x_i^2 f_i} \quad (6)$$

$$d_l = \sum x_i l_i = \sum \left( x_i \frac{x_i f_i}{\sum x_i f_i} \right) = \frac{\sum x_i^2 f_i}{\sum x_i f_i} \quad (7)$$

$$d_n = \sum x_i n_i = \sum \left( x_i \frac{f_i}{\sum f_i} \right) \quad (8)$$

where  $f_i$  is the number of particles within the given size range ( $x_i, x_i+\Delta x$ ), and the parameters  $m_i, a_i, l_i$  and  $n_i$  are size distribution functions by mass, area, chord length, and number of the particles, respectively. If the particles are non-spherical, shape factor should be applied in the equations as well. It can be seen from Eqs. (5)-(8) that the contribution of small size particles is more and more pronounced to the mean diameter from  $d_m$  through  $d_n$ . In other words, compared with the mass mean diameter, the small size particles play a more important role in the determination of number mean diameter. For instance, for a packed bed with spheres of three diameters (1.5mm, 3mm and 6mm) at the mass ratio of 1:1:1, the resulting mean diameters are as shown in Table 2. In this case, mass mean diameter is two times of number mean diameter. From the mass mean diameter (3.5mm) to the number

mean diameter (1.73mm), it is getting closer to the diameter of the smallest spheres (1.5mm).

Table 2. Different mean diameters of a packed bed

<b>Spheres</b>	<b>Mass ratio</b>	$d_m$ (mm)	$d_a$ (mm)	$d_l$ (mm)	$d_n$ (mm)
1.5mm+3mm+6mm	1:1:1	3.5	2.57	2	1.73

When confronted with so varied mean diameters, a natural question is that which one is suitable for coolability analysis of a debris bed? So far there has not been a clear answer yet. On the one hand, mass and area mean diameters were widely applied in coolability studies. For instance, Konovalikhin [12] used mass mean particle diameter in the tests on packed beds with sand grains, and found that the experimental dryout heat flux agrees with the prediction of the Lipinski's model. Similarly, mass mean particle diameter was employed by Schmidt [14], while area mean particle sizes were used by Dhir [21]. On the other hand, a so-called effective diameter was proposed and used in coolability studies [10-11]. The effective particle diameter is usually derived from experimental data of fluid flow in porous media provided that the above-mentioned friction laws are still valid. For DCC-2 rubbles bed [10], the effective diameter (1.42mm) is much smaller than the mass mean diameter (2.43mm). For the STYX particle bed [11], it was found the effective particle diameter is close, but not equal to the number mean diameter. Zeisberger & Mayinger [22] performed an investigation on a porous bed filled with steel balls (4mm) and glass spheres (0.95mm), yielding pressure gradient closer to the model prediction by using number mean diameter rather than area mean diameter.

In general, the literature survey shows that number mean diameter is seemingly more suitable for debris characterization than mass and area mean diameters, but the data are still quite limited. The present study is to advance the understanding of the effective particle diameters of particulate beds packed with varied size distributions of particles. The work consists of three folds: i) to obtain the effective diameter of a so-packed bed via single-phase flow experiments; ii) to compare the effective diameter with the mean diameters obtained by Eqs.(5)-(8); and iii) to examine the validity of the effective diameter in two-phase flow modeling. The item #i is realized by the measurement of pressure gradients of gas/water single-phase flow through the packed beds. The item #ii is conducted to see if the effective diameter can be represented by the number mean diameter; if not, which one of the mean diameters is close in the first place. Item #iii is performed to confirm the applicability of the effective particle diameter to coolability assessment.

The experiment is carried out on the POMECO-FL test facility, as illustrated in Fig. 3, which is basically an adiabatic water/air single- and two-phase flow loop for porous media. Major components of the test facility are made of transparent Plexiglas to facilitate visual observation. The test section accommodating the particulate bed is made of a Plexiglas pipe with the inside diameter of 90mm and the height of 635mm. Four annular chambers for pressure tapping are designed to surround the pipe at different levels, with radial holes (0.5mm in diameter) uniformly distributed as opening from the bed to the annular chambers. The chambers do not only provide an average pressure reading over the entire circumference of each tapping point, but also prevent gas and particles from entering the impulse lines of pressure transducers. At both the inlet and the outlet of the test section, two pieces of stainless steel wire mesh are applied between the flanges to support the bed from below and prevent the particles from leaving the bed. Air is supplied from the bottom and

flows up through the packed bed, but water can be supplied from either the bottom or the top for a bottom-fed (co-current flow) or a top-flooding (counter-current flow) bed.

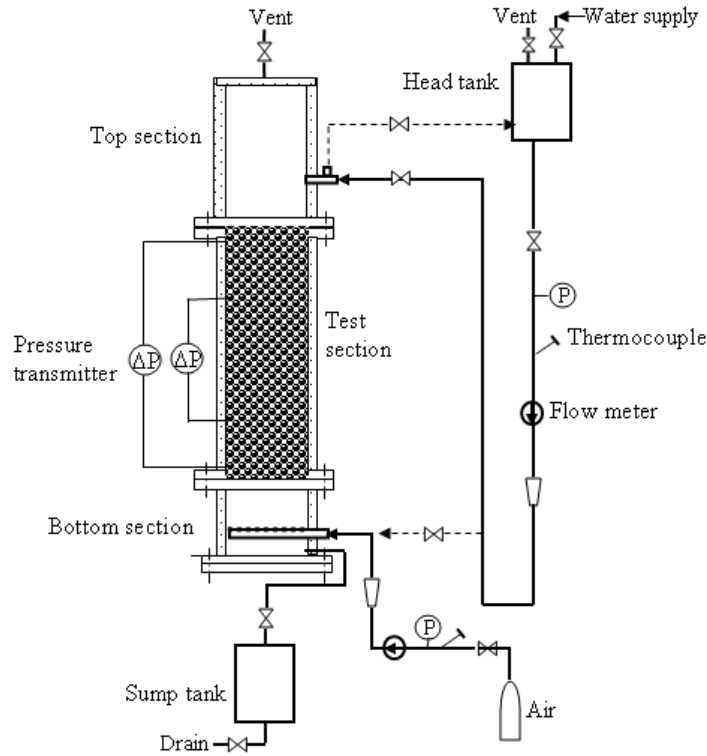


**Fig. 3:** The schematic diagram of POMECO-FL facility.

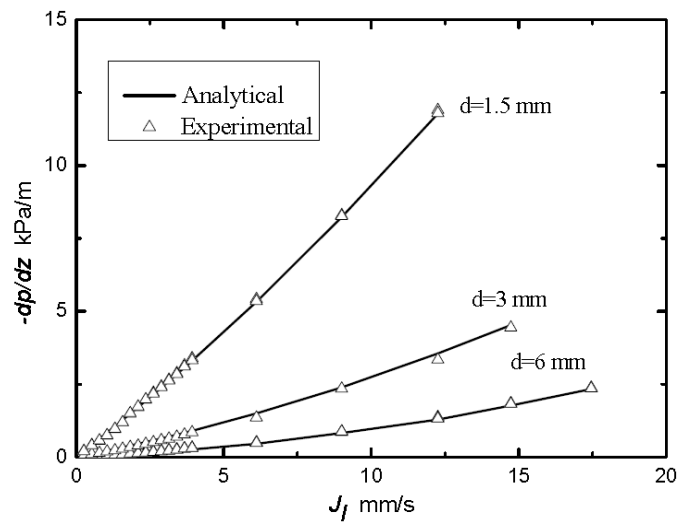
Two Rosemount-3051 differential pressure transmitters with high accuracy are mounted on the test section to measure entire and half pressures drops, respectively, of single or two-phase flow through the bed. Valve manifolds are used with the differential pressure transmitters to perform the block, equalizing and vent requirements of the transmitters. The flowrates of gas and water flows are measured by seven OMEGA flowmeters with different measuring ranges. The pressure and temperature are monitored by using OMEGA pressure transducers and K-type thermocouples. The flowmeters and pressure transducers were calibrated prior to experiment. A Data Acquisition System (DAS) is realized via National Instruments data acquisition products and a computer program written in LabView. The program collects the data from thermocouples, pressure transducers, flowmeters (via manual input), and employs the indicators to show the numerical data and its graphical representation such as charts.

Since the models for coolability analysis are sensitive to the bed porosity as well as the particle size, yielding results from coolable to non-coolable situation with a relatively small change in the two parameters [11], a great care is taken here in determining the bed porosity. This is achieved by accurate measurement of the material density (double check and verification of factory data) and the particle mass (free of moisture) loaded into the bed. The porosity is then determined by

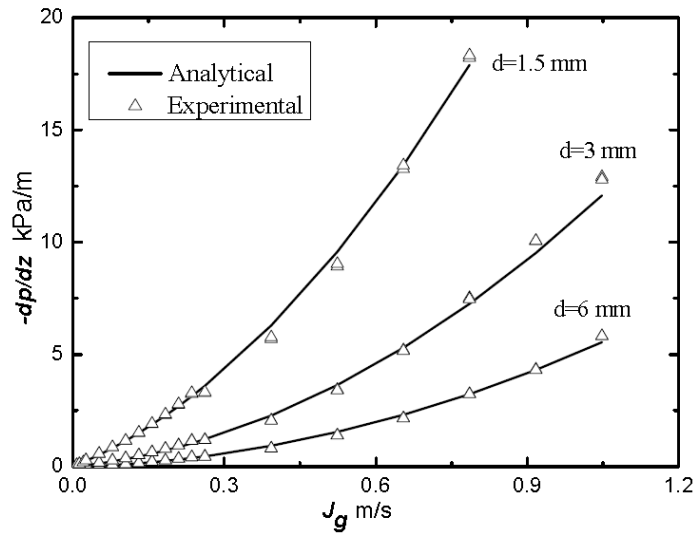
$$\varepsilon = 1 - \frac{\sum M_j / \rho_j}{V_0} \quad (9)$$

where  $\varepsilon$  is the porosity of the bed,  $M_j$  is the mass of the particles made of material  $j$  and  $V_o$  is the total volume the bed occupies (including void). The particles are well mixed prior to filling in the test section so that a uniform packed bed can be obtained.

In addition to the calibration of instrumentation, the test facility and its measurement system were also qualified by measurements of single-phase flow through three beds packed with single-size glass spheres of diameter 1.5mm, 3mm and 6mm, respectively. Water and air were employed as working fluid, respectively. The measured pressure gradients were then compared with those predicted by the Ergun's equation, whose predictions are generally accepted for packed beds of spheres with satisfactory accuracy. Fig. 4 shows the comparison between the measured data the analytical results of Ergun's equation, where triangle symbols represent experimental data, and the solid curves are analytical results. The quality of experimentation and instrumentation can be ensured by the good agreement.



(a) water flow



(b) air flow

**Fig. 4:** Pressure gradients of fluid flow through packed beds with single-size spheres.

The multi-size particles used in the beds are glass spheres (cf. Fig. 5), with the diameter ranging from 0.7mm to 10mm. The particulate beds chosen in the present study are as shown in Table 3, in which  $d_n$ ,  $d_l$ ,  $d_a$  and  $d_m$  are mean diameters of particles based on their distribution in number, length, surface area and mass (see Eqs.5-8), respectively. The effective particle diameter  $d_e$  is derived from the experimental data. Reynolds number ( $Re$ ) is defined as

$$Re = \frac{\rho \cdot j \cdot d_{sd}}{\mu(1 - \varepsilon)} \quad (10)$$

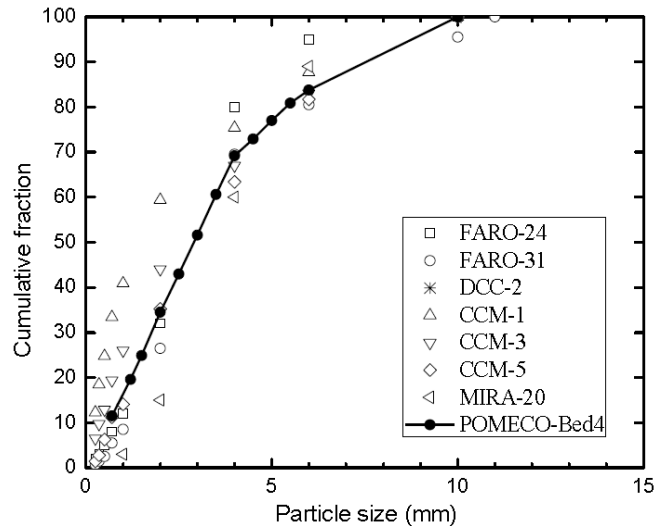
where  $j$  and  $d_{sd}$  are the superficial velocity of fluid and Sauter mean diameter of the particles, respectively. Bed-1, Bed-2 and Bed-3 are packed with two-diameter spheres, while Bed-4 is composed of multi-diameter spheres whose size distribution is as shown in Fig. 6 and Table 4.

Table 3. Test beds packed with mixture of multi-diameter spheres.

Bed	Diameters (mm)	Mass ratio / Fraction	Porosity $\varepsilon$	$d_n$ (mm)	$d_l$ (mm)	$d_a$ (mm)	$d_m$ (mm)	$Re$	$d_e$ (mm)
1	1.5+3	1:1	0.34	1.67	1.8	2	2.25	<7	1.98
								>7	1.82
2	1.5+6	1:1	0.31	1.57	1.76	2.4	3.75	<7	2.16
								>7	1.71
3	1.5+6	4:1	0.33	1.52	1.57	1.76	2.4	<7	1.77
								>7	1.58
4	0.7-10	See Fig. 6 and Table 4	0.34	0.9	1.18	2.12	3.97	<7	1.82
								>7	1.22



Fig. 5: Spheres used in the packed beds.



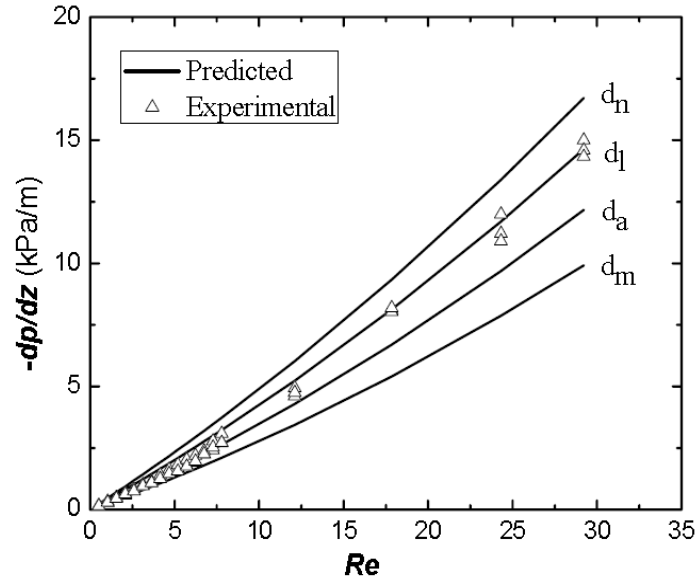
**Fig. 6:** Particle size distributions in FCI test with real corium [23] and in Bed-4.

Table 4. Particle size distribution of Bed-4.

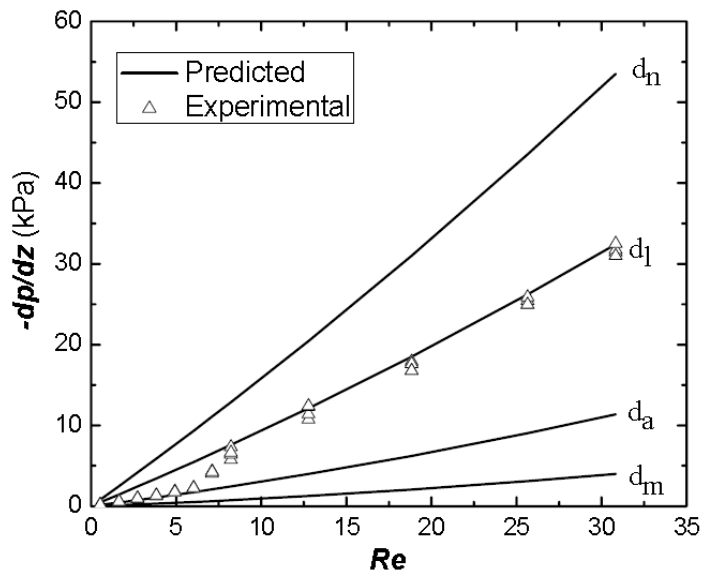
Particle size (mm)	Accumulative fraction
0.7	11.5
1.2	19.6
1.5	24.9
2	34.5
2.5	43.0
3	51.6
3.5	60.6
4	69.2
4.5	72.9
5	77
5.5	80.9
6	83.8
10	100

Fig. 7a shows the pressure gradients of single-phase flow in Bed-1 increase with increasing Reynolds number, where the triangle marks are the measured values, while the solid curves are predicted by Ergun's equation using the mean particle diameters mentioned above. Notably, at low Reynolds number ( $Re < 7$ ) the pressure gradient predicted by Ergun equation using area mean diameter of the particles is comparable with the experimental data. This means that the area mean diameter can be employed as the effective particle diameter for the bed. However, as the Reynolds number increases to a threshold value ( $Re > 7$ ), the length mean diameter is more representative of the effective particle diameter. As shown in Table 1, the same conclusion is applicable to Bed-2 and Bed-3 that are all packed with two-diameter spheres as well.

For Bed-4 packed with multi-diameter spheres, the effective particle diameter is also varied with increasing Reynolds number, as depicted in Fig. 7b. When the Reynolds number is small ( $Re < 7$ ), the effective particle diameter of the spheres is not equal but relatively close to area mean diameter. For high Reynolds number ( $Re > 7$ ), the effective particle diameter is almost the same as the length mean diameter.



(a) Bed-1



(b) Bed-4

**Fig. 7:** Measured pressure gradients single-phase flow in the particle beds and predicted values by Ergun's equation using various mean particle diameters of the bed.

For understanding of the friction law of two-phase flow through a particulate bed packed with multi-size particles, an investigation on pressure drop of air-water two-phase flow through Bed-4 was carried out. Fig. 8 shows the experimental data are comparable with the predictions of Reed's model, given the effective particle diameter obtained from above.

In summary, the effective particle diameters can be represented by the area mean diameters of the particles in the beds at low flowrate ( $Re < 7$ ), while at high velocity ( $Re > 7$ ) the effective particle diameters are closer to the length mean diameters. The measured pressure drops of two-phase flow through the particulate beds have a good agreement with predictions of Reed's model.

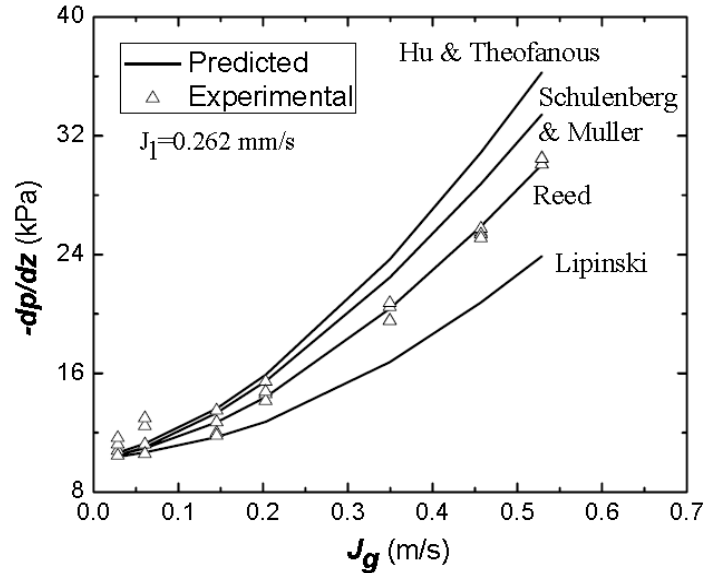


**Fig. 8:** Measured pressure gradients of two-phase flow in Bed-4 and predicted values by Ergun's equation using various mean particle diameters of the bed.

## 2.2. Steam explosion energetics

The objective of the steam explosion study at KTH is to pursue new evidences of corium low explosivity by performing MISTEE experiments. The new focus during 2009 is to perform MISTEE experiment with eutectic and non-eutectic single oxidic molten droplet.

Previously, single drop steam explosion experiments were conducted with a metallic melt (tin) on the MISTEE test facility [24-26], to pursue a basic understanding of micro-interactions in steam explosion. The anatomy of the explosion was realized by a diagnostic system named SHARP [24] which enables synchronized visualization of both bubble dynamics and melt evolution during the explosion period, granting first-of-a-kind data on micro-interactions in droplet explosion. The experimental results show that the vapor film dynamics experiences three distinct cycles of bubble expansion and collapse, and melt preconditioning (deformation/pre-fragmentation of a molten drop immediately following the pressure trigger) is instrumental to the subsequent coolant entrainment and resulting energetics of the so-triggered steam explosion [25].

To reduce the properties gap between the corium and its simulant, the MISTEE test facility was upgraded to be able to work with oxidic materials at high melting temperatures. The modifications include development and procurement of high-temperature crucible and delivery system, new high-speed camera, new triggering system for high pressure shock high-temperature thermocouples and pyrometer. The first step of experiment [27] was to find a ceramic type binary oxide with liquidus temperature not higher than 1400°C because of some limitations of the facility. After testing of different oxidic materials (e.g.,  $\text{MoO}_3\text{-Bi}_2\text{O}_3$ ,  $\text{MnO-TiO}_2$ ,  $\text{MoO}_3\text{-ZrO}_2$ ,  $\text{MnO-MoO}_3$ ,  $\text{MoO}_3\text{-TiO}_2$ ), the binary mixture of  $\text{WO}_3\text{-Bi}_2\text{O}_3$  (whose phase diagram is shown in Fig. 9) was selected to perform single droplet steam explosion experiment. 12 testss were performed with this mixture, in which 5 were in

a eutectic composition (27:73 mol%,  $T_{\text{liquidus}}=870^{\circ}\text{C}$ ) and 7 in a non-eutectic composition (27:73 mol%,  $T_{\text{liquidus}}=890^{\circ}\text{C}$ ), with water temperatures varying from  $20^{\circ}\text{C}$  to  $80^{\circ}\text{C}$ . Unfortunately, this particular material had very peculiar characteristics (cf. Figs. 10 & 11): very fine fragments, similar to a thin powder, were left behind during the droplet plunging into the water, making it impossible to resolve the bubble dynamics. Moreover, the probable droplet disintegration would influence the melt preconditioning and thus the energetics of the interaction. The fact that most of the experiments rendered energetic steam explosions even under low subcooled conditions, strengthen such possibility. For these reasons, the  $\text{WO}_3\text{-Bi}_2\text{O}_3$  was not considered as a suitable simulant for the current study.

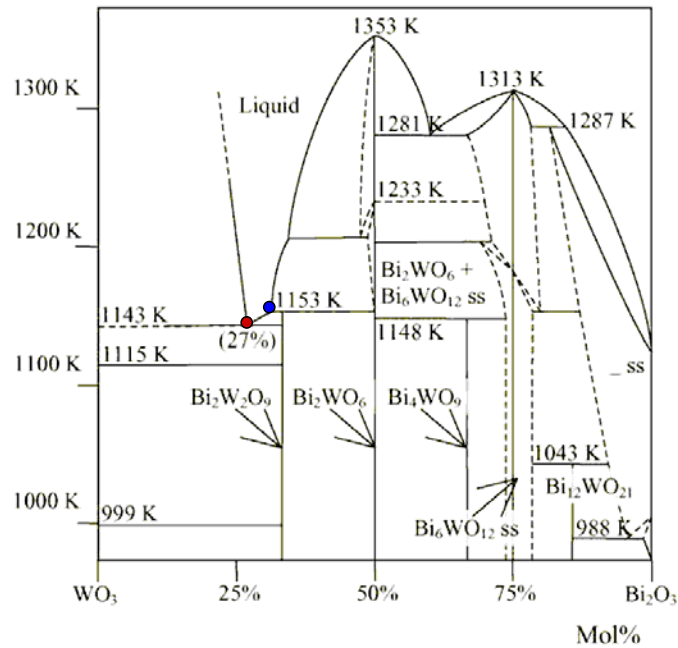


**Fig. 9:** Phase diagram of  $\text{WO}_3\text{-Bi}_2\text{O}_3$ .

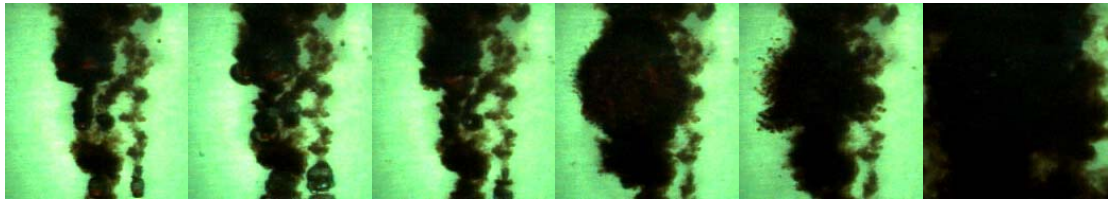


**Fig. 10:**  $\text{WO}_3\text{-Bi}_2\text{O}_3$  eutectic mixture undergoing an energetic steam explosion and fine fragmentation of the molten material.

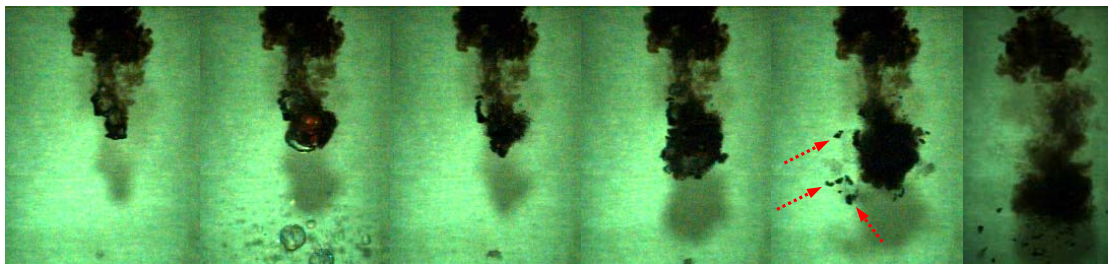


**Fig. 11:**  $\text{WO}_3\text{-Bi}_2\text{O}_3$  non-eutectic mixture undergoing a mild steam explosion and coarse fragmentation of the molten droplet.

Finally, the binary oxide mixture of  $\text{WO}_3$ -CaO has been chosen as the corium simulant. Its phase diagram is as shown in Fig. 12. Total 37 experiments using  $\text{WO}_3$ -CaO were performed on the MISTEE test facility, being 32 of an eutectic composition (75:25 mol%,  $T_{\text{liquidus}}=1135^\circ\text{C}$ ,  $\Delta T_{\text{superheat}}\sim 200\text{-}300^\circ\text{C}$ ) and 5 experiments with a non-eutectic composition (72:27 mol%,  $T_{\text{liquidus}}=1232^\circ\text{C}$ ,  $T_{\text{solidus}}=1135^\circ\text{C}$ ,  $\Delta T_{\text{superheat}}\sim 200^\circ\text{C}$ ), under high subcooled conditions. However, only 12 eutectic tests and 3 non-eutectic tests (see Table 5) were chosen for the analysis due to their data completeness, e.g. simultaneous record of bubble and melt dynamics, and the absence of non-condensable gases.

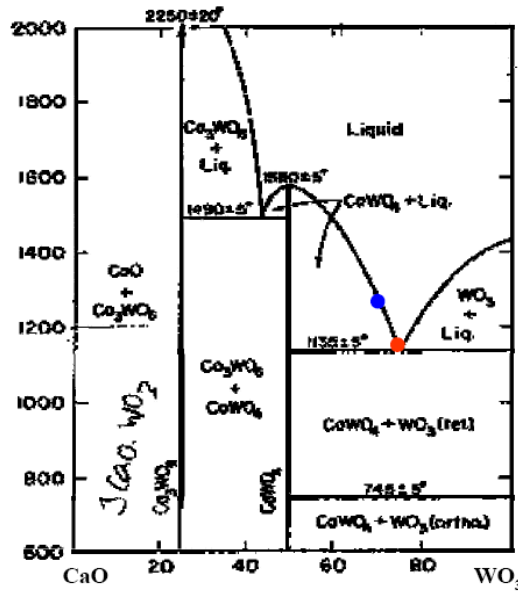


Fig. 12: Phase diagram of  $\text{WO}_3$ -CaO.

As established by the previous experiments with tin, the steam explosion micro-interactions are depicted by the vapor film and melt dynamics, in which melt preconditioning and conversion ratio will be evaluated.

Table 5. Test matrix.

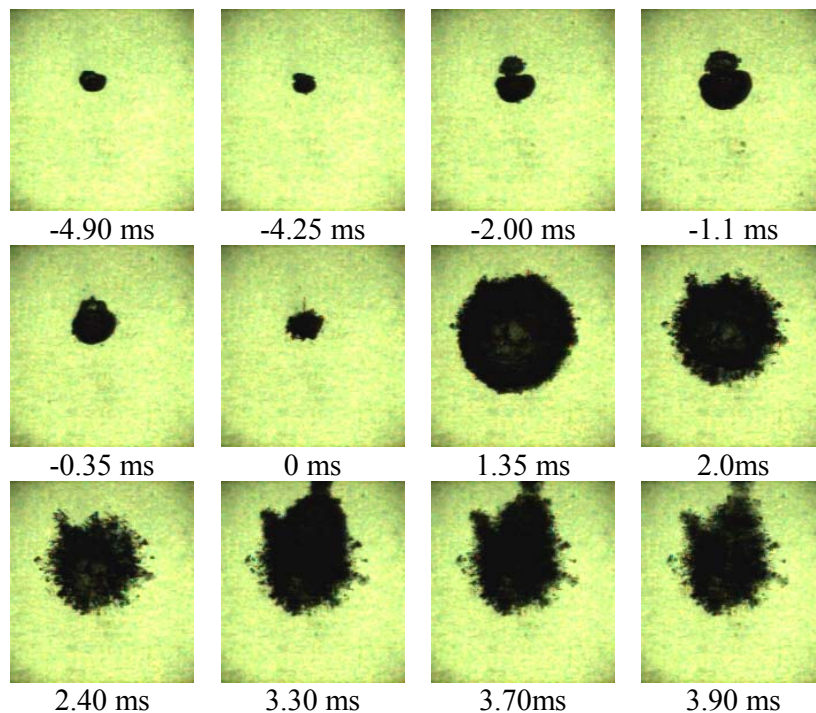
Material ( $\text{WO}_3$ -CaO)	Experiment no.	$T_{\text{melt}}$	$T_{\text{coolant}}$
Eutectic	21	1400	20.4
	22	1350	21.1
	23	1350	20
	24	1350	22
	25	1350	19.2
	26	1350	20.4
	27	1350	21.2
	28	1350	21.4
	29	1350	20.5
	30	1450	21.8
	31	1450	24.4
	32	1400	24.5
Non-eutectic	2	1480	23.4
	3	1480	20.1
	4	1480	24.1

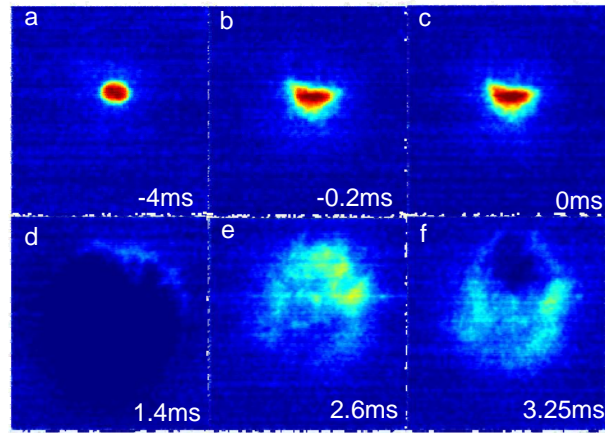
### 2.2.1. Bubble and melt dynamics

Still photographic pictures, with a temporal resolution of 0.05 ms per frame, are presented in the top of Figs. 13-16; and the x-ray radiography pictures, with a temporal resolution of 0.05 ms per frame 0.2 ms, are presented in the bottom of Figs. 13-16. The images reveal the vapor film and melt progression during the steam explosion of  $\sim 1$  g of eutectic and non-eutectic molten  $\text{WO}_3\text{-CaO}$  under high water subcooling.

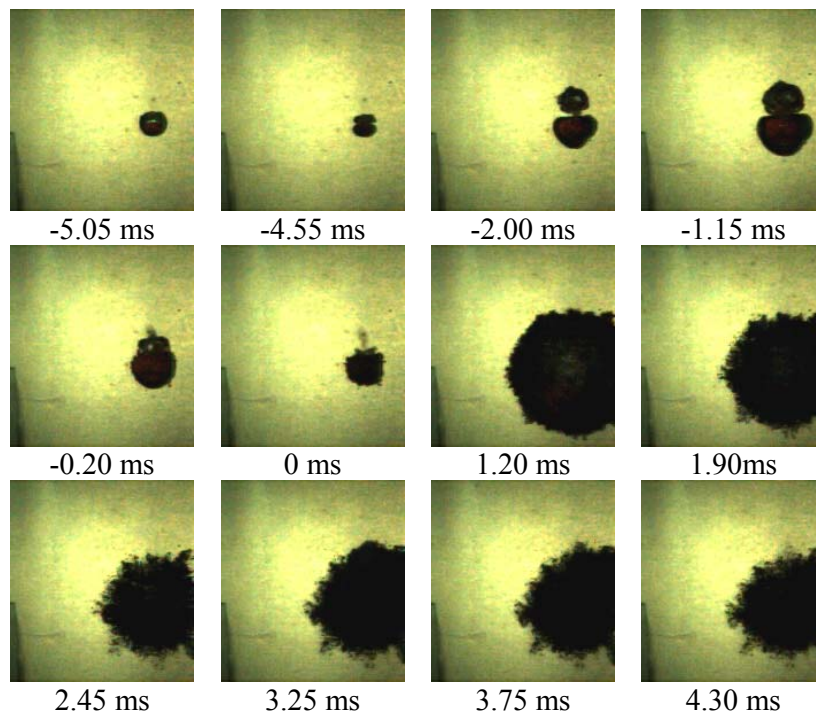
Similar to the single droplet experiments performed with a metallic melt (tin), the vapor film dynamics produces three defined cycles of bubble expansion and collapse.

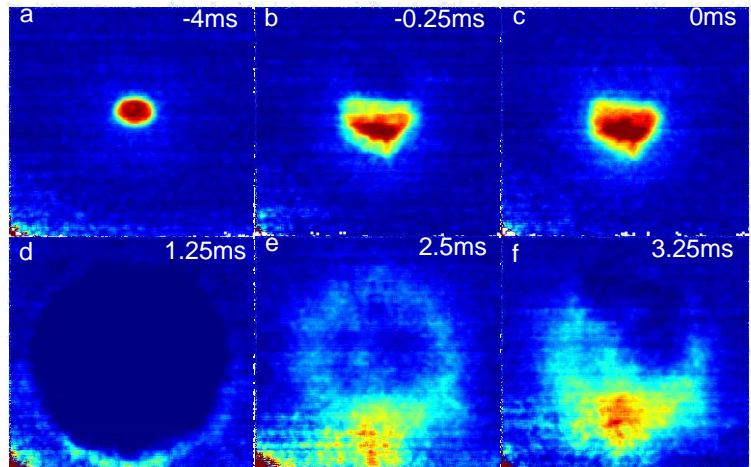
Due to the melt's high temperature, a vapor film with a small dome on the rear side is immediately formed at the time when the molten  $\text{WO}_3\text{-CaO}$  droplet enters the water, and endures as it descends into the water. The interaction initiates when the external pressure wave destabilizes the vapor film, triggering the parallel oscillatory behavior of the rear and cyclic jet formation underneath of the main bubble. The near liquid-liquid contact occurs and nucleation takes place expanding the bubble and rear. To this point, the vapor film dynamics creates complex internal flows which lead to the deformation/ prefragmentation of the melt droplet. That can be clearly seen in the radiographic images, in which the initial elliptical droplet, Figs. 13a-16a (bottom), evolves into a convoluted droplet with fine fragments present in the droplet's periphery, Figs. 13b-16b (bottom). The overgrown bubble/rear reaches its maximum and starts to collapse towards the molten droplet. The accelerating interface hits the molten droplet, adding the coolant into the interaction zone; at this point ( $t=0$  ms), the actual direct melt-coolant contact takes place. Explosive bubble expansion and fine fragmentation of the melt droplet is then accomplished in the subsequent two cycles.



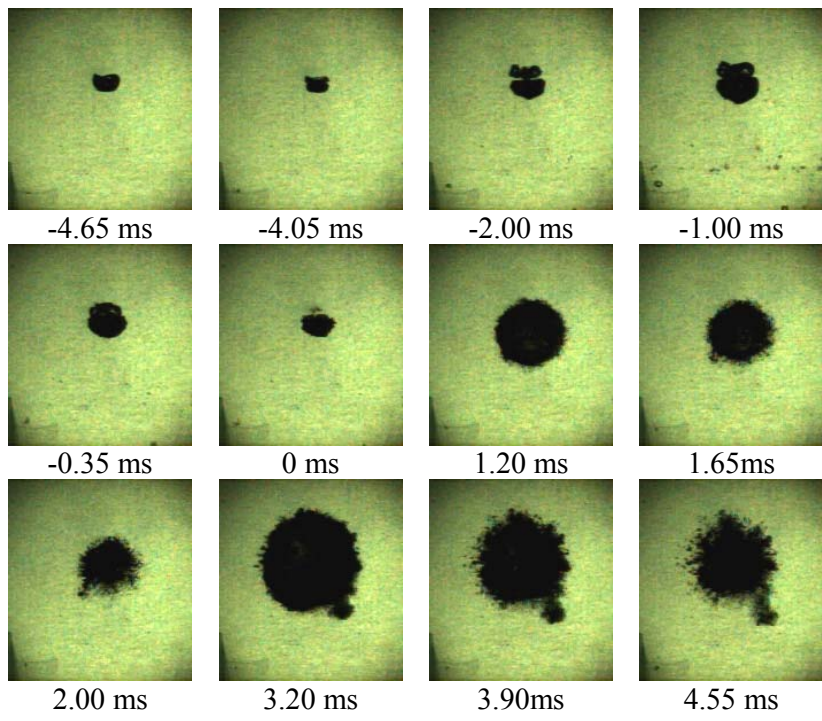


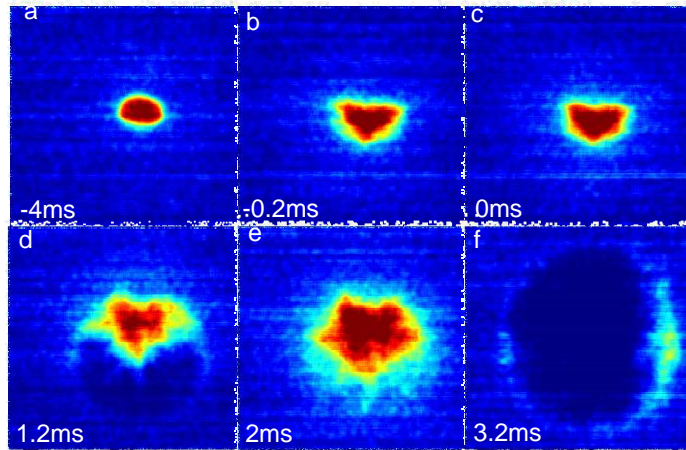
**Fig. 13:** Vapor film and melt dynamics of a 0.9194g of eutectic  $\text{WO}_3\text{-CaO}$  (Initially at  $1350^\circ\text{C}$  in water at  $20.4^\circ\text{C}$  undergoing steam explosion).



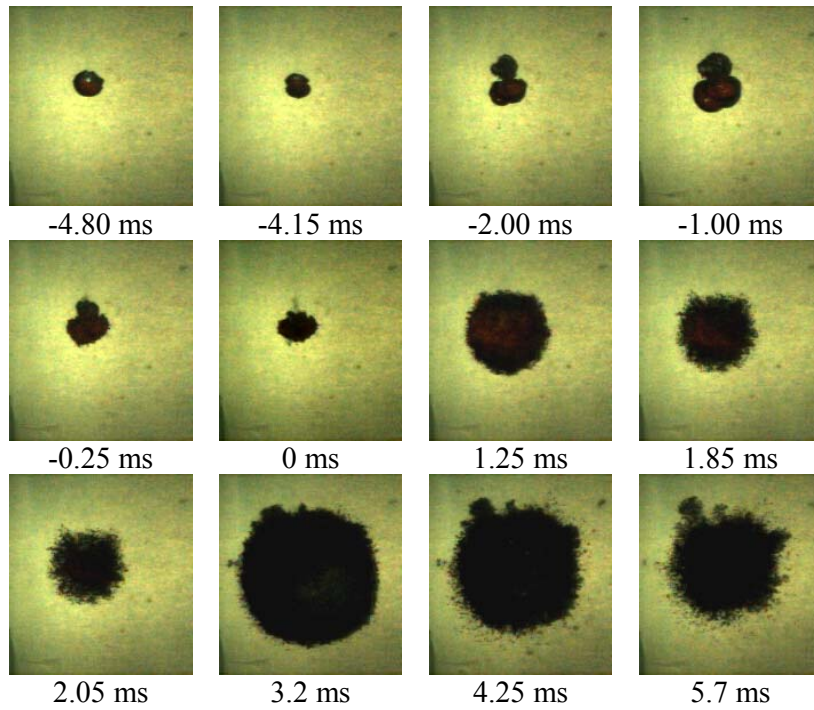


**Fig. 14:** Vapor film and melt dynamics of a 1.0463g of non-eutectic  $\text{WO}_3\text{-CaO}$  (Initially at  $1480^\circ\text{C}$  in water at  $20.1^\circ\text{C}$  undergoing steam explosion).





**Fig. 15:** Vapor film and melt dynamics of a 0.9611g of eutectic  $\text{WO}_3\text{-CaO}$  (Initially at  $1350^\circ\text{C}$  in water at  $20.2^\circ\text{C}$  undergoing steam explosion).



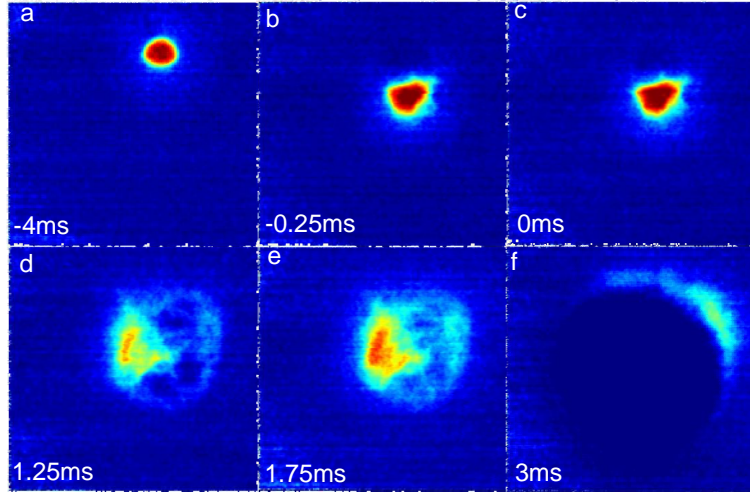


**Fig. 16:** Vapor film and melt dynamics of a 0.9474g of non-eutectic  $\text{WO}_3\text{-CaO}$  (Initially at  $1480^\circ\text{C}$  in water at  $24.1^\circ\text{C}$  undergoing steam explosion).

What was not observed in the tin experiments is that whenever the first cycle expansion is underdeveloped, the second cycle expansion is also suppressed consequently, but it is then compensated by generating an outsized third expansion; see Figs. 15-16.

One could rationalize such singularity by understanding the dynamics of the first cycle since it establishes the initial conditions for the energetic second cycle. The first cycle is mainly affected by two major aspects: coolant/melt temperature (vapor film stability) and vapor film morphology (asymmetry); which in turn affect the melt preconditioning. Since all the experiments with oxidic material were performed under similar coolant/melt temperature, we turn our attention to the vapor film morphology.

During the hot melt droplet trajectory in the water, the vapor film forms a small dome on the rear of the droplet. Its presence plays an important role when disturbed by the external pressure wave (similar to the interaction when non-condensable gases are present). Such asymmetry leads to complex pressure dynamics governing the bubble's internal flows and jet formation on its interface. The resulting forces and interactions are sufficient to disturb the droplet surface, facilitating its preconditioning.

The increased preconditioned droplet adds heat to the growing bubble, which is translated to a larger 1<sup>st</sup> cycle expansion, Fig. 18a. At this point, the overgrown bubble will then collapse, reaching a high impact velocity; this setting added to the highly preconditioned droplet facilitates the melt-coolant mixing, generating an energetic second cycle, Fig. 18b. The opposite is also true, if a droplet melt presents a diminutive vapor rear, the preconditioning will be lesser, the first cycle will be less prominent, which will then lead to a less energetic second cycle. The later implies an ineffective melt fragmentation, leading to a larger residual melt, as shown in Figs. 15e-16e (bottom), which is responsible for the third extensive expansion.

Given the experimental work on the two different eutectic and non-eutectic materials, no evident dissimilarity in the vapor film, Fig. 17, or melt history was found for the actual melt droplet superheat ( $200^{\circ}\text{C}$ ).

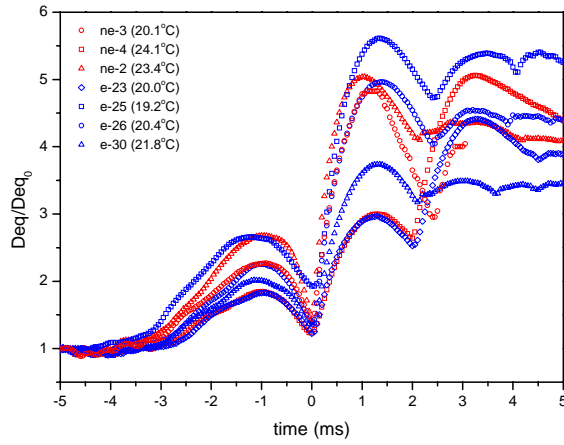


**Fig. 17:** Radial history of eutectic and non-eutectic  $\text{WO}_3\text{-CaO}$  single droplet.

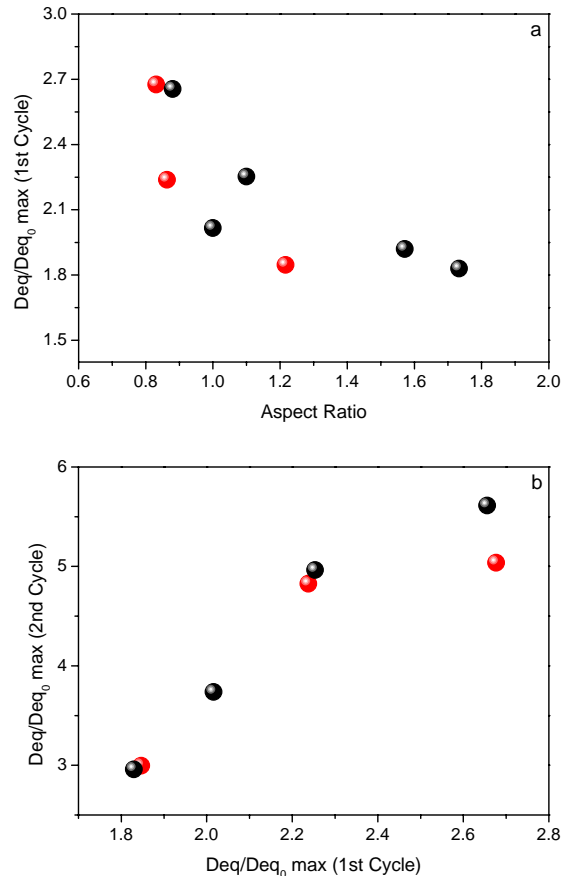


**Fig. 18:** (a) Vapor film aspect ratio in respect to the 1<sup>st</sup> cycle maximum radial; (b) Expansion 1<sup>st</sup> and 2<sup>nd</sup> cycle maximum radial expansion.

## 2.2.2. Steam explosion energetics

From the bubble radial history, one can estimate the work done by the expanding bubble and thus the steam explosion conversion ratio. One should keep in mind that it is not possible to estimate the third cycle conversion ratio due to the fragments dispersed in the coolant, which disables the possibility to identify of the vapor film volume. That is to say, in the cases in which the third cycle is the more energetic, the contribution to the total energetics will not be fairly represented. However, the correlation with the preconditioning will be conserved, i.e. the higher the preconditioning the higher the second cycle conversion ratio, as seen in Fig. 19. Yet, no apparent differences between the eutectic and no-eutectic material, in terms of steam explosion energetics and preconditioning, can be discerned. This may be due to the high superheat employed in the experiments.

The phase change of a binary oxide melt droplet, e.g. solidification and/or formation of a mushy phase, typically occurs over a specific temperature range, which is determined by the *liquidus* and *solidus* line. Accordingly, if the droplet superheat is high enough, the material phase will be kept far above the liquidus line, i.e. in liquid form, until the initiation of the interaction<sup>1</sup>. Thus, the actual experiments are probably away from the region in which solidification behaviors would play a role on the steam explosion energetics, see Fig. 20.

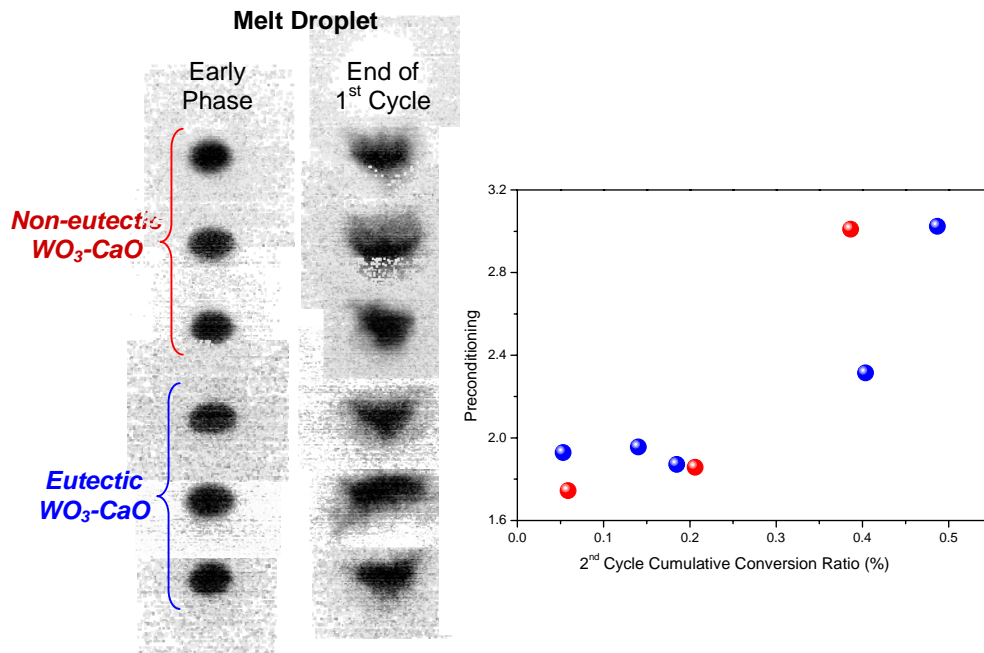


**Fig. 19:** Melt droplet preconditioning and 2<sup>nd</sup> cycle cumulative conversion ratio.

A failed experiment (ne-5), in which the melt was delivered earlier than intended due to a leak in the crucible, is shown in Fig. 21. Although the exact melt temperature is not known,

<sup>1</sup> The TROI experiments had a high initial superheat, yet the UO<sub>2</sub>-ZrO<sub>2</sub> melt mixture could be transformed quickly into a non-liquid form due to the high radiative heat flux, which leads to fast crust and/or of mushy zone formation.

it certainly has a lower superheat than the tests above presented and analyzed. In this particular case a crust formation is visible during fragmentation (1.75 ms). It was not possible to estimate the energetics, but it is clear that the interaction was milder than the experiments presented in Figs. 13-16, given that the fine fragmentation is diminutive. The presence of the crust and suppression of a third cycle implies the presence of less material available for a steam explosion.

In order to identify the material effect threshold, i.e. when mushy phase would start playing a role, one would need to perform experiments with lower superheat to develop a solidification behavior map for non-eutectic melts and its influence on the steam explosion energetics.

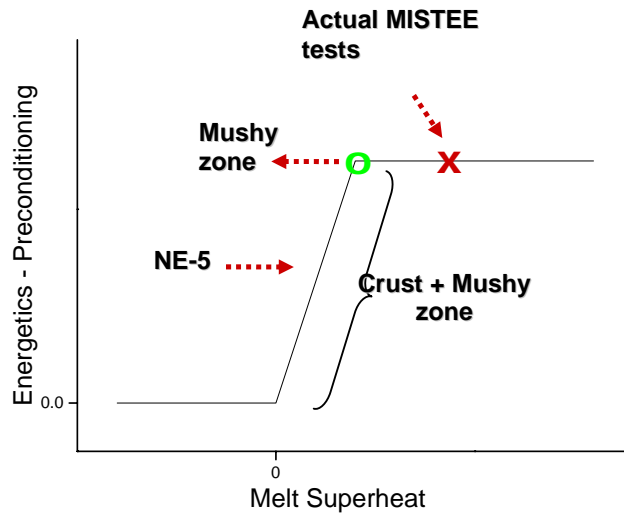


**Fig. 20:** Melt droplet energetics/ preconditioning in respect to melt superheat and possible solidification behavior.

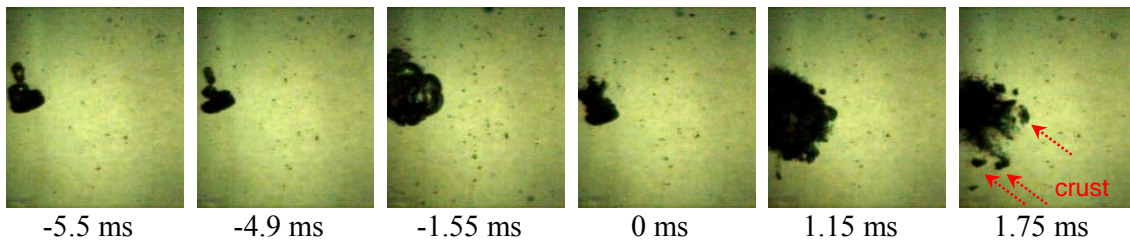


**Fig. 21:** Vapor film dynamics of a 1.2g of non-eutectic  $WO_3$ -CaO, in water at  $24.6^\circ C$  undergoing a mild steam explosion (crust presence): NE-5.

### 2.2.3. Metallic (tin) versus Oxidic ( $WO_3$ -CaO) materials

Although one should not quantitatively compare the bubble and melt dynamics of the oxidic ( $WO_3$ -CaO) experiments with the metallic (Tin) experiments due to difference in the water subcooling (the highest subcooling for the tin experiments is around  $55^\circ C$ , while for the

oxide tests the subcooling was around 70°C), Table 6 shows no major difference between the tests.

Moreover, features inherent from the metallic test, e.g. spontaneity of the steam explosion, can be justified by the lower temperature of the droplet melt which in turn will produce a less stable vapor film susceptible to external disturbances.

The above mentioned arguments reinforce the idea the oxidic melt droplets were in a complete liquid state by the time that the steam explosion is initiated.

Table 6. Some features from the Tin and WO<sub>3</sub>-CaO experiments

	<b>Tin Experiments</b>	<b>WO<sub>3</sub>-CaO Experiments</b>
<i>Vapor Film Morphology</i>	Diminutive Vapor Dome (0.8 -1.6)	Pronounced Vapor Dome (0.8 -1.6)
<i>1<sup>st</sup> Cycle Deq<sub>max</sub>/D<sub>o</sub></i>	1.8 – 2.7	1.8 – 2.7
<i>Preconditioning A<sub>final</sub>/A<sub>initial</sub></i>	1 – 2.7	1.8 – 3.0
<i>2<sup>nd</sup> Cycle Deq<sub>max</sub>/D<sub>o</sub></i>	3 – 4	3 – 5.8
<i>Energetics Up to the 2<sup>nd</sup> Cycle</i>	0.3 – 0.44	0.14 – 0.5
<i>2<sup>nd</sup> Cycle Deq<sub>max</sub>/D<sub>o</sub></i>	3.5 - 5	3.5 – 5.4

### 3. Concluded Remarks

Significant progress was made and important findings were obtained in the INCOSE project during year 2009. Substantial advances in process modeling and new insights into related mechanisms were gained from studies on i) corium coolability in the BWR lower head by integral and coupled assessment for taking into account the CRGT cooling as a potential SAM measure; ii) debris bed coolability with focus on characterization of the effective particle diameter of multi-size particles as found in debris beds; and iii) micro dynamics (anatomy) of a single oxidic droplet steam explosion.

Specifically, method for coupling of ECM/PECM models with RELAP5 was developed to enhance predictive fidelity for melt pool heat transfer. MELCOR was employed to examine the CRGT cooling efficiency by considering an entire accident scenario. For a particulate bed packed with multi-size particles, the effective particle diameter can be represented by the area mean diameter of the particles, while at high velocity ( $Re > 7$ ) the effective particle diameter is closer to the length mean diameter. The pressure drop of two-phase flow through the particulate bed can be predicted by Reed's model. The steam explosion experiments using oxidic mixture of WO<sub>3</sub>-CaO show that there is no apparent difference in steam

explosion energetics and preconditioning between the eutectic and no-eutectic materials, probably due to high superheat (200°C) of the melt applied in the tests. More achievements and detailed descriptions can be found in the related publications listed in References. Overall, the research of the INCOSE project in 2009 has advanced the knowledge of steam explosion and in-vessel coolability in BWRs.

As we enter 2010, the project continues data generation and methodology development, in order to reduce uncertainty in quantification of corium melt risk in a hypothetical reactor severe accident of LWRs. Specifically, in the in-vessel coolability topic we will continue ECM/PECM application for melt pool heat transfer and develop a coupled analysis method of CFD-structural mechanics (melt pool convection-vessel behavior), in order to reduce uncertainty in prediction of penetration (IGT) failure on the vessel. We will continue POMECO-FL tests for friction laws of particle beds with prototypical debris characteristics, and construct POMECO-HT test facility for coolability qualification of such beds, and development and validation of related simulation tools. In steam explosion topic, MISTEE experiments with the oxidic binary mixture ( $\text{WO}_3\text{-CaO}$ ) will be performed at lower superheat, since the material effect might be perceived at lower superheat, where mechanisms like the mushy zone will start playing a role. Methodology will be developed for steam explosion risk assessment under reactor application.

## References

- [1] C.T. Tran and T.N. Dinh, The Effective Convectivity Model for simulation of melt pool heat transfer in a light water reactor pressure vessel lower head. Part I: Physical processes, modeling and model implementation, *Progress in Nuclear Energy*, **51** (8), pp.849-859, 2009.
- [2] C.T. Tran and T.N. Dinh, The Effective Convectivity Model for simulation of melt pool heat transfer in a light water reactor pressure vessel lower head. Part II: Model assessment and application, *Progress in Nuclear Energy*, **51** (8), pp.860-871, 2009.
- [3] C.T. Tran and T.N. Dinh, Simulation of core melt pool formation in a reactor pressure vessel lower head using Effective Convectivity Model, *Nuclear Engineering and Technology*, **41** (7), pp.929-944 2009.
- [4] C.T. Tran, P. Kudinov and T.N. Dinh, An approach to numerical simulation and analysis of molten corium coolability in a BWR lower head, *Nuclear Engineering and Design, Nuclear Engineering and Design*, Article in press, doi:10.1016/j.nucengdes.2009.11.029
- [5] C.T. Tran, The Effective Convectivity Model for simulation and analysis of melt pool heat transfer in a light water reactor pressure vessel lower head, Doctoral Thesis in Energy Technology, Royal Institute of Technology, Stockholm, Sweden 2009.
- [6] C.T. Tran and P. Kudinov, The effective convectivity model for simulation of molten metal layer heat transfer in a boiling water reactor lower head, Proc. of ICAPP'09, Shinjuku Tokyo, Japan, May 10-14, 2009.
- [7] F. Cadinu, T.C. Thanh and P. Kudinov, Analysis of in-vessel coolability and retention with control rod guide tube cooling in boiling water reactors, NEA/SARNET2 Workshop - In-Vessel Coolability, NEA Headquarters, Issy-les-Moulineaux, France, October 12-14, 2009.
- [8] W.M. Ma and C.T. Tran, On the Effectiveness of CRGT cooling as a severe accident management measure for BWRs, Proc. of OECD/NEA Workshop on Implementation

- of Severe Accident Management Measures, Villigen, Switzerland, October 26-28, 2009.
- [9] G. Hofmann, On the location and mechanisms of dryout in top-fed and bottom-fed particulate beds, *Nuclear Technology*, **65**: 36–45, 1984.
- [10] A. W. Reed, E. D. Bergeron et al, “Coolability of UO<sub>2</sub> debris bed in pressurized water pools: DCC-1 and DCC-2 experiment results”, *Nuclear Engineering and Design*, **97**: 81-88, 1985.
- [11] I. Lindholm, S. Holmström, J. Miettinen, V. Lestinen, J. Hyvärinen, P. Pankakoski, H. Sjövall, Dryout heat flux experiments with deep heterogeneous particle bed, *Nuclear Engineer and Design*, **236**, 2060–2074, 2006.
- [12] M. J. Konovalikhin, Investigations on melt spreading and coolability in a LWR severe accident, *Ph. D thesis of Royal Institute of Technology*, Stockholm, November 2001.
- [13] K. Hu and T.G. Theofanous, On the measurement and mechanism of dryout in volumetrically heated coarse particle beds, *Int. J. Multiphase Flow*, **17** (4): 519-532, 1991.
- [14] W. Schmidt, Influence of multidimensionality and interfacial friction on coolability of fragmented corium, *PhD thesis of Universität Stuttgart*, German, 2004.
- [15] W.M. Ma and T.N. Dinh, The effects of debris bed’s prototypical characteristics on corium coolability in a LWR severe accident, *Nuclear Engineering and Design*, **240** (3), pp. 598-608, 2010.
- [16] S. Ergun, Fluid flow through packed columns, *Chemical Engineering Progress*, **48** (2): 89-94, 1952.
- [17] R.J. Lipinski, A one dimensional particle bed dryout model. *ANS Transactions*, **38**, 386-387, 1981.
- [18] A.W. Reed, The effect of channeling on the dryout of heated particulate beds immersed in a liquid pool. PhD thesis, Massachusetts Institute of Technology, Cambridge, 1982.
- [19] T. Schulenberg and U. Müller, An improved model for two-phase flow through beds of coarse particles, *Int. J. Multiphase flow*, **13** (1): 87-97, 1987.
- [20] S. L. Soo, *Multiphase Fluid Dynamics*, New York: Science press Gower Technical, 1990.
- [21] V.K. Dhir, Boiling and two-phase flow in porous media, *Annual Review of Heat Transfer*, **5**: 303-350, CRC Press, Boca Raton, 1994.
- [22] A. Zeisberger, F. Mayinger, Heat transport and void fraction in granulated debris, *Nuclear Engineering and Design*, **236**: 2117–2123, 2006.
- [23] I. Lindholm, A review of Dryout heat fluxes and coolability of particle beds, SKI report 02:17, 2002.4.
- [24] R.C. Hansson, H.S. Park, T.N. Dinh, Simultaneous high speed digital cinematographic and X-ray radiographic imaging of an intense multi-fluid interaction with rapid phase changes, *Experimental Thermal and Fluid Science*, **33**, pp 754-756, 2009.
- [25] R.C. Hansson, H.S. Park, T.N. Dinh, Dynamics and preconditioning in a single droplet vapor explosion, *Nuclear Technology*, **167**, pp 223-234, 2009.
- [26] R.C. Hansson, Triggering and energetics of a single drop vapor explosion: the role of entrapped non-condensable gases, *Nuclear Engineering and Technology*, **41** (9), pp.1215-1222, 2009.
- [27] *Proc. of the 28<sup>th</sup> Review Meeting for Project “Melt-Structure-Water Interactions in a Severe Accident”* (MSWI-28), KTH, Stockholm, Sweden, June 10, 2009, 84p.
- [28] *Proc. of the 29<sup>th</sup> Review Meeting for Project “Melt-Structure-Water Interactions in a Severe Accident”* (MSWI-29), KTH, Stockholm, Sweden, December 9, 2009, 90p.

Title	In-vessel Coolability and Steam Explosion in Nordic BWRs
Author(s)	Weimin Ma, Roberta Hansson, Liangxing Li, Pavel Kudinov, Francesco Cadinu, Chi-Thanh Tran
Affiliation(s)	Royal Institute of Technology (KTH), Sweden
ISBN	978-87-7893-289-1
Date	May 2010
Project	NKS-R / INCOSE
No. of pages	28
No. of tables	6
No. of illustrations	21
No. of references	28
Abstract	<p>The INCOSE project is to reduce the uncertainty in quantification of steam explosion risk and in-vessel coolability in Nordic BWR plants with the cavity flooding as a severe accident management (SAM) measure. During 2009 substantial advances and new insights into physical mechanisms were gained for studies of: (i) in-vessel corium coolability – development of the methodologies to assess the efficiency of the control rod guide tube (CRGT) cooling as a potential SAM measure; (ii) debris bed coolability – characterization of the effective particle diameter of multi-size particles and qualification of friction law for two-phase flow in the beds packed with multi-size particles; and (iii) steam explosion – investigation of the effect of binary oxides mixture’s properties on steam explosion. An approach for coupling of ECM/PECM models with RELAP5 was developed to enhance predictive fidelity for melt pool heat transfer. MELCOR was employed to examine the CRGT cooling efficiency by considering an entire accident scenario, and the simulation results show that the nominal flowrate (~10kg/s) of CRGT cooling is sufficient to maintain the integrity of the vessel in a BWR of 3900 MWth, if the water injection is activated no later than 1 hour after scram. The POMEKO-FL experimental data suggest that for a particulate bed packed with multi-size particles, the effective particle diameter can be represented by the area mean diameter of the particles, while at high velocity (<math>Re &gt; 7</math>) the effective particle diameter is closer to the length mean diameter. The pressure drop of two-phase flow through the particulate bed can be predicted by Reed’s model. The steam explosion experiments performed at high melt superheat (&gt;200oC) using oxidic mixture of WO<sub>3</sub>-CaO didn’t detect an apparent difference in steam explosion energetics and preconditioning between the eutectic and non-eutectic melts. This points out that the next step of MISTEE experiment will be conducted at lower superheat.</p>
Key words	severe accident, debris coolability, steam explosion